Marita L. Rodriguez
Department of Mechanical Engineering,
University of Washington,
Seattle, WA 98195

Brandon T. Graham
Department of Bioengineering,
Washington State University,
Pullman, WA 99164

Lil M. Pabon
Department of Pathology,
Center for Cardiovascular Biology,
Institute for Stem Cell and
Regenerative Medicine,
University of Washington,
Seattle, WA 98109;
Department of Bioengineering,
University of Washington,
Seattle, WA 98195

Sangyoon J. Han
Department of Cell Biology,
Harvard University,
Cambridge, MA 02115

Charles E. Murry
Department of Pathology,
Center for Cardiovascular Biology,
Institute for Stem Cell and
Regenerative Medicine,
University of Washington,
Seattle, WA 98109;
Department of Bioengineering,
University of Washington,
Seattle, WA 98195;
Department of Medicine/Cardiology,
University of Washington,
Seattle, WA 98195

Nathan J. Sniadecki[1]
Department of Mechanical Engineering,
University of Washington,
Seattle, WA 98195;
Department of Bioengineering,
University of Washington,
Seattle, WA 98195
e-mail: nsniadec@uw.edu

Measuring the Contractile Forces of Human Induced Pluripotent Stem Cell-Derived Cardiomyocytes With Arrays of Microposts

Human stem cell-derived cardiomyocytes hold promise for heart repair, disease modeling, drug screening, and for studies of developmental biology. All of these applications can be improved by assessing the contractility of cardiomyocytes at the single cell level. We have developed an in vitro platform for assessing the contractile performance of stem cell-derived cardiomyocytes that is compatible with other common endpoints such as microscopy and molecular biology. Human induced pluripotent stem cell-derived cardiomyocytes (hiPSC-CMs) were seeded onto elastomeric micropost arrays in order to characterize the contractile force, velocity, and power produced by these cells. We assessed contractile function by tracking the deflection of microposts beneath an individual hiPSC-CM with optical microscopy. Immunofluorescent staining of these cells was employed to assess their spread area, nucleation, and sarcomeric structure on the microposts. Following seeding of hiPSC-CMs onto microposts coated with fibronectin, laminin, and collagen IV, we found that hiPSC-CMs on laminin coatings demonstrated higher attachment, spread area, and contractile velocity than those seeded on fibronectin or collagen IV coatings. Under optimized conditions, hiPSC-CMs spread to an area of approximately 420 μm^2, generated systolic forces of approximately 15 nN/cell, showed contraction and relaxation rates of 1.74 μm/s and 1.46 μm/s, respectively, and had a peak contraction power of 29 fW. Thus, elastomeric micropost arrays can be used to study the contractile strength and kinetics of hiPSC-CMs. This system should facilitate studies of hiPSC-CM maturation, disease modeling, and drug screens as well as fundamental studies of human cardiac contraction. [DOI: 10.1115/1.4027145]

Introduction

In the past decade, heart disease has become the leading cause of death worldwide and has continued to be a major economic burden to developed countries [1]. However, recent research suggests that stem cells may be the key to understanding, treating, and even reversing heart disease [2,3]. Investigators have used human cardiomyocytes derived from stem cells (hSC-CMs) as a model system to study the developmental and pathological states of the heart at the cellular level [4–8]. hSC-CMs have also been used to screen new pharmacological treatments for heart disease [4,5,9]. In addition, recent findings suggest that hSC-CMs, when infused or injected into damaged heart tissue, can partially restore heart function by supplanting the dead or diseased tissue [8,10–15]. Therefore, the applications for hSC-CMs in cardiovascular medicine are vast. Of the currently available sources of human stem cells, human induced pluripotent stem cells (hiPSCs) hold tremendous promise due to their easy availability, high proliferation rates in culture, potential to serve as a source of patient-specific cardiomyocytes, and, unlike human embryonic stem cells (hESC), their use is noncontroversial.

One of the most important functional characteristics of a cardiomyocyte is its ability to produce contractile forces; therefore, the ability to quantify this contraction would provide a powerful assessment tool for performing studies with stem cell-derived

[1]Corresponding author.

Contributed by the Bioengineering Division of ASME for publication in the Journal of Biomechanical Engineering. Manuscript received August 21, 2013; final manuscript received February 21, 2014; accepted manuscript posted March 10, 2014; published online April 10, 2014. Assoc. Editor: Kevin D. Costa.

cardiomyocytes. However, assessing the contractile properties of hiPSC-CMs is a difficult task. In vitro methods that have been previously used to measure the contractility of single cardiomyocytes include: magnetic beads [16], polyacrylamide gels [17–20], carbon fiber deflection [21–24], atomic force microscopy [25–27], optical edge detection [28,29], flexible cantilevers [30], and strain gauges [31]. However, many of these techniques are two-point force assays, meaning that the cell is suspended between a surface and a force transducer, and twitch forces can be measured only along a single axis. Current protocols used to derive hiPSC-CMs yield cells with relatively immature and unaligned cytoskeletons, which contract along multiple different directions. Therefore, two-point force assays are unable to fully capture the twitch force produced by immature cell types. Furthermore, while adult cardiomyocytes primarily attach to surfaces at their distal ends, immature cardiomyocytes, like hiPSC-CMs, form integrin attachments along their basal surface [32]. Thus, a technique that limits the attachment of immature cells to two distinct regions of the cell also limits the amount of integrin attachments that these cells can form. Additionally, some of these techniques require clamping, gluing, or poking of the cell, which could affect its ability to produce force. Others are computationally complex or require mathematical estimations in order to determine twitch forces [17–20]. The contractile properties of a population of cardiomyocytes have also been approximated by seeding these cells within a three-dimensional construct [33–39]. However, in this configuration, it is difficult to determine the actual contractile force produced by individual cells, since a portion of this contraction is lost to the rigidity of the bulk tissue and/or through its cell-cell contacts. Moreover, due to the tightly packed configuration of cells and extracellular matrix (ECM) within these constructs, it is only possible to determine the average mechanical properties of the cells, and the properties of unique subpopulations of cardiomyocytes are lost. Lastly, the nonplanar, thick, three-dimensional environment of multicellular constructs makes it difficult to use microscopy to analyze individual cells within the construct.

Micropost arrays have been shown to effectively measure the contractile forces produced by neonate [40] and adult rat cardiomyocytes [41,42]. Furthermore, high-speed imaging of individual post deflections by IonOptix systems has enabled the measurement of the contractile velocity and power produced by these cells [43,44]. More recently, a modification on this platform enabled the measurement of the contractile forces produced by human embryonic stem cell-derived cardiomyocytes (hESC-CMs) [45]. These studies have established that the micropost platform is a viable means for assessing the contractile properties of various types of cardiomyocytes. Here, we demonstrate a significant improvement in micropost technology by simultaneously measuring the contractile force, velocity, and power produced by hiPSC-CMs at each of their adhesion points. This approach consists of culturing cells on arrays of silicone microposts, imaging them, and assessing their contractile properties using a custom written MATLAB. Cells adhered to the microposts were also immunofluorescently stained to investigate structural markers of maturation.

Previous studies have suggested that there are developmental differences between neonate and adult cardiomyocytes in regard to the recognition of different extracellular matrix proteins. Neonate rat cardiomyocytes have been found to attach and spread on collagen types I through V, fibronectin, and laminin [32,46]. Alternatively, adult rat cardiomyocytes have been found to preferentially attach to laminin and type IV collagen whereas they weakly attach to fibronectin-coated surfaces and do not attach at all to interstitial collagens I and III [32,46–48]. However, the influence that these matrix proteins have on hiPSC-CM attachment remains unclear. Thus, for our initial studies, we investigated the effect that ECM protein coating has on the attachment, as well as the contractile and structural maturation, of hiPSC-CMs on microposts.

Methods

Micropost Substrate Preparation. Arrays of silicone microposts were fabricated by casting polydimethylsiloxane (PDMS) from silicon wafers with patterned SU-8 structures via soft lithography, as previously described [49]. Each micropost in the array was 2.3 μm in diameter, 7.2 μm in height, and had 6 μm center-to-center spacing. The arrays of PDMS microposts were cast onto #1 round glass coverslips with a diameter of 25 mm. The tips of the microposts were coated via microcontact printing with either 50 μg/ml of mouse laminin (Life Technologies), human fibronectin (BD Biosciences), or human collagen IV (Millipore), while the remaining surfaces of the micropost array were fluorescently stained with bovine serum albumin conjugated with Alexa Fluor 594 and blocked with 0.2% Pluronic F-127 in phosphate buffer solution [50].

Cell Culture. Human iPSCs derived from the IMR-90 lung fibroblast cell line (Thomson and Wisconsin-Madison) [51] were propagated under feeder-free conditions. High density monolayers of these stem cells were then differentiated into cardiomyocytes by sequential treatment of activin A and bone morphogenetic protein 4 [52], supplemented at the early stages of differentiation with the Wnt agonist CHIR 99021 and Wnt antagonist Xav 939. Cardiomyocytes were cultured on Matrigel-coated plates in RPMI medium: RPMI 1640 with L-glutamine (Gibco), supplemented with 1X B-27 (Gibco) and 1% penicillin/streptomyosin (Cellgro). This media was exchanged every other day. A large number of beating cardiomyocytes were observed in the culture approximately 14 days after induction and were studied between 40 and 70 days later. Prior to experimentation, these cells were dissociated from their culture surfaces with a solution of 0.25% trypsin ethylenediaminetetra-acetic acid (Cellgro) in Versene^{TM} (Gibco). Dissociated cells were then seeded onto micropost arrays at a density of approximately 500,000 cells per 25 mm diameter substrate in RPMI medium supplemented with 5% fetal bovine serum. The following day, the media was removed and replaced with serum-free RPMI medium, which was exchanged every other day. Prior to imaging, the micropost coverslips were transferred into an Attoflour® viewing chamber (Life Technologies), and cell media were replaced with HEPES RPMI medium (Gibco).

Cell Contractility Analysis. One week following cell seeding onto the microposts, individual hiPSC-CM muscle twitches were recorded using high-speed video microscopy. A phase contrast video was taken in the optical plane at the tips of the microposts to track the movement of a post during twitch contractions, and a fluorescent image was taken in the plane at the base of the microposts to establish the reference position for each post (Fig. 1(*a*)). A Hamamatsu ORCA-Flash2.8 Scientific CMOS camera fitted on a Nikon Eclipse Ti upright microscope was used to acquire these images at 60× magnification using a water immersion objective. This camera and microscopy setup is able to record images at frame rates over 100 frames per second, depending on the size of the selected region of interest. Additionally, a live cell chamber was used to maintain the cells at 37 °C throughout the imaging process. To determine micropost deflections over time, a custom-written MATLAB code was used to locate and track the centroid of each micropost, using grayscale and binary imaging tools (Fig. 1(*b*)). The position of a micropost tip was then compared to the position of its base, for each of the captured images (Fig. 1(*c*)). The difference in the position of these centroids is the deflection of the micropost at that particular instance in time. Figure 1(*d*) shows the position of these centroids for an individual micropost during a twitch event, where a plus sign indicates the position of the bottom of the micropost, and the centroid of the post area represents the position of the tip of the micropost. This deflection can then be plotted over multiple twitch events with the same MATLAB code, and the twitch force can be calculated by

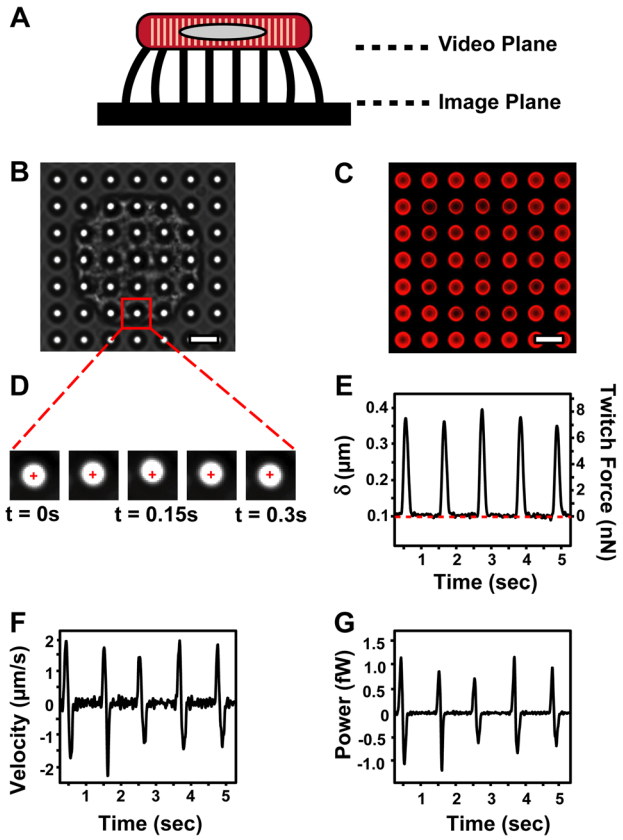

Fig. 1 Technique the twitch force, velocity, and power of a single hiPSC-CM is determined by seeding cells onto a micropost array, selecting a beating cell of interest, and then taking a high-speed video of the post tips, as well as a reference image of the post bases (*a*). This video is taken in the phase contrast setting (*b*), while the reference image is taken in the red fluorescent channel (*c*). A custom MATLAB code is then used to determine the location of each post's centroid in the reference plane (plus sign), as well as it is used to track the location of the post's centroid in the video plane (*d*). The difference in location between these two centroids over time gives the deflection of the post over multiple twitch events, which can be multiplied by the post stiffness to yield the twitch force (*e*). Here, the dashed line represents the passive tension measured for this post. This deflection data can then be used to determine the twitch velocity (*f*), and power (*g*) of that post. Scale bars represent 6 μm.

multiplying the temporal deflection data by the bending stiffness of the micropost (Fig. 1(*e*)),

$$F_i = k\delta_i \tag{1}$$

where F_i is the force at a single micropost in frame i of the captured image sequence, k is the bending stiffness of the post (27.83 nN/μm), and δ_i is its deflection in frame i. Assuming that each micropost can be modeled as a cantilever beam that is fixed at one end, and undergoes small deflections at the other, the stiffness can be calculated using beam bending theory [50],

$$k = \frac{3\pi E D^4}{64 L^3} \tag{2}$$

where D is the diameter (2.3 μm), E is the Young's modulus (2.9 MPa), and L is the length (7.2 μm) of each micropost. Using the same MATLAB code, the velocity of a micropost at a given time point is calculated from (Fig. 1(*f*)),

$$V_i = \frac{\delta_{i+1} - \delta_{i-1}}{t_{i+1} - t_{i-1}} \tag{3}$$

where t represents the time elapsed from the start of the video. In turn, twitch force and twitch velocity at a given time point can be multiplied together to obtain the twitch power for an individual micropost beneath the cell (Fig. 1(*g*)),

$$P_i = F_i V_i \tag{4}$$

From this data, the total force produced by a single cell was determined by summing the absolute magnitudes of the force measured at each post beneath the cell. Twitch force is calculated as the difference between the passive force, i.e., the resting tension, and the average peak force measured during each twitch event, while force per area is the twitch force divided by the spread area of the cell. Values of maximum twitch velocity reported in this work were determined by comparing the maximum contraction and relaxation velocities measured at each post beneath a cell, and then averaging these values across multiple beats. Values of contraction and relaxation twitch power were calculated at each time point by multiplying the force and velocity of each micropost for an image frame and summing these values for all posts beneath the cell.

Immunofluorescence and Image Analysis. Two days after seeding hiPSC-CMs onto micropost arrays, cell counts were taken, using phase microscopy, from 20 equivalent regions on each micropost substrate. These counts were then normalized against those obtained for the fibronectin-coated microposts within each of the three separate experiments, and were averaged to yield an overall attachment percentage. This imaging was performed using a Nikon Ti Eclipse inverted microscope with live cell imaging chamber, which kept the cell environment at 37 °C.

After live experiments, the cells were fixed and stained in order to image their myofibril structure on top of the posts. Prior to fixing, a Triton extraction protocol was used to permeabilize the samples [43,53]. Briefly, samples were submerged for 10 s in a buffer containing 10 mM PIPES (J.T.Baker), 50 mM NaCl (BDH), 150 mM sucrose (J.T.Baker), 2 mM phenylmethylsulfonyl fluoride (Electron Microscopy Sciences), 3 mM MgCl (BDH), 20 μg/ml aprotinin (G-Biosciences), 1 μg/ml leupeptin (G-Biosciences), and 1 μg/ml pepstatin (G-Biosciences) with a pH of 6.5. The samples were then placed in the same buffer for 2 min, with the addition of 0.5% Triton X-100. Following Triton extraction, the samples were fixed in 4% paraformaldehyde (EMD Chemicals) in phosphate buffered solution. Cell nuclei were then stained with Hoechst 33342 (Life Technologies) and sarcomeric α-actinin was treated with monoclonal mouse anti-α-actinin (Sigma Aldrich) and stained with goat antimouse AlexaFluor 488 (Life Technologies).

Once fluorescent images were taken, NIS Elements software was used to manually measure sarcomere lengths and Z-band widths, as well as cell circularity and spread area (inset of Fig. 5(*a*)). For Z-band width analysis, at least five Z-bands were selected at random from the α-actinin stained image of the cell, and their lengths were measured using the NIS Elements 2 Points Length tool. These values were averaged to get an overall average Z-band length for each cell. Using the same tool, the average sarcomere length for each cell was determined by measuring the horizontal distance between the midpoints of two parallel Z-bands. At least two measurements of sarcomere length were measured per cell. Circularity, which is a measure of how round an object is, was calculated as follows:

$$C = \frac{4\pi A}{p^2} \tag{5}$$

where A is the area of the cell and p is the length of its perimeter. The values for area and perimeter used in this calculation were determined by manually tracing around the image of the cell with the NIS Elements Polygon Area tool. Alternatively, cell area

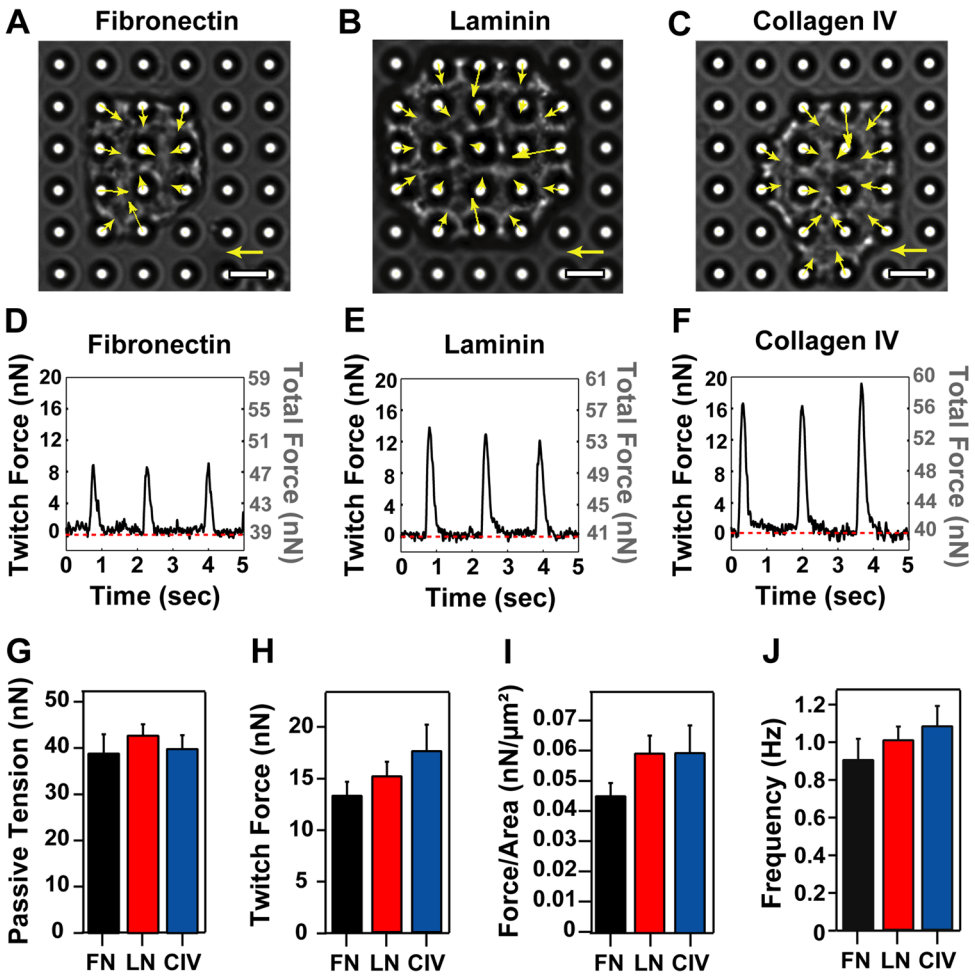

Fig. 2 Twitch force representative images of hiPSC-CMs on fibronectin (*a*), laminin (*b*), and collagen IV (*c*) at peak twitch force indicate that the highest forces are present along the edges of the cell, and that the majority of the cell's force is directed towards the cell center. Here, the arrows indicate the direction and magnitude of the force at each post. When the magnitude of these individual force vectors are summed, the total force produced by the cell can be plotted over multiple twitch cycles. Representative force traces for hiPSC-CMs on fibronectin (*d*), laminin (*e*), and collagen IV (*f*) demonstrate that the micropost array platform is capable of capturing these twitch cycles with high temporal resolution. Here, the text on the left of the graph indicates the twitch force, while that on the right indicates total force, and the dashed line indicates the passive force produced by the cell. Quantification of the passive force (*g*), maximum twitch force (*h*), and force per area (*i*), for hiPSC-CMs on different ECM proteins revealed that the quantities are statistically similar across all three conditions. Additionally, there was no significant difference in the spontaneous beating rate of the cells on the three different ECM proteins (*j*). Scale bar represents 6 μm and scale arrow indicates 6 nN.

measurements used in the force per area calculations were taken from a screenshot of the recorded phase contrast videos (Fig. 1(*b*)) to ensure proper matching between cell area and force production. Only the areas of cells with measurable beating forces were used for the overall average spread area calculation.

Statistical Analysis. Due to the nonparametric nature of the data, statistical differences between fibronectin, laminin, and collagen IV groups were determined with a Kruskal–Wallis ANOVA on Ranks. To compare multiple treatments, a Mann–Whitney post hoc test with a Bonferroni correction was performed. Normality of the data distributions was determined by the Ryan Joiner test. Statistical significance was assessed at $p < 0.05$, and statistical differences against fibronectin are indicated by an asterisk, while those against collagen IV are indicated by a numerical sign. Data in the text are reported as the mean ± standard error of the mean. Error bars in bar graphs also represent standard error of the mean.

Results

Contractile Force, Velocity, and Power. The twitch force, maximum twitch velocity, and twitch power produced by a cardiomyocyte are key determinants of the cell's contractile maturation. To determine the contractile maturation of human iPSC-CMs, the cells were seeded onto micropost arrays that had been microcontact printed with fibronectin, laminin, or collagen IV. The total forces produced at each post underneath a cell were analyzed from video microscopy (Figs. 2(*a*)–2(*c*)) to determine the passive tension, twitch force, force per area, and frequency of these cells. Upon investigating the passive tension produced by cells from each of the three conditions, we found no statistical differences between any of the ECM groups (Fig. 2(*g*)).

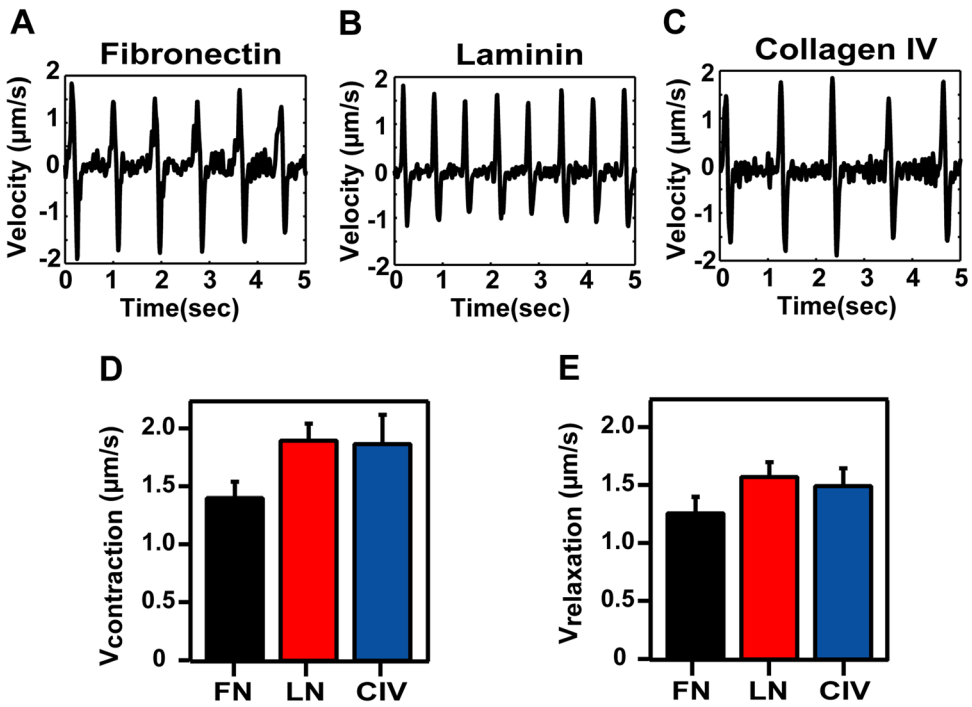

Fig. 3 Twitch velocity representative maximum velocity traces for hiPSC-CMs on fibronectin (*a*), laminin (*b*), and collagen IV (*c*) indicate that the micropost platforms is capable of capturing both the contraction and relaxation velocity produced by spontaneously beating cells. Quantification of these traces revealed higher overall contraction and relaxation velocities for cells on collagen IV, but no significant difference between any of the treatments (*d*) and (*e*).

Additionally, we observed that the twitch force produced by hiPSC-CMs was lowest on fibronectin-stamped posts (13.34 nN), followed by laminin (15.23 nN) and then collagen IV (17.64 nN) (Fig. 2(*h*)), although there were no significant differences in these values. Similarly, force per area measurements for cells on the three different ECMs were not statistically different from one another (Fig. 2(*i*)). Moreover, there were no significant differences in the spontaneous beating frequency of the cells on all three ECM proteins, although cells on laminin or collagen IV tended to have higher beating frequencies (Fig. 2(*j*)).

Each twitch contraction of the hiPSC-CMs had two distinct phases, a contraction phase and a relaxation phase. These phases can be seen in representative curves of the velocity for cells seeded on each of the three ECM proteins (Figs. 3(*a*)–3(*c*): fibronectin, laminin, and collagen IV). From the start of the contraction phase, the contraction velocity speeds up, reaches a maximum value, and then decreases back down to zero when the maximum twitch force is reached. Here, this maximum value in the velocity is identified as the contraction velocity. Similarly, during relaxation, the cell contraction speed starts at zero, decreases to some negative maximal value, and then returns to zero until the next twitch contraction commences. The greatest negative velocity reached during this phase is henceforth referred to as the relaxation velocity. The maximum twitch velocities averaged between 1.4 to 2.0 μm/s for contraction and 1.2 to 1.6 μm/s for relaxation across multiple experiments, with no significant differences in either parameter seen when comparing the three ECM groups (Figs. 3(*d*) and 3(*e*)). The velocities obtained for cells on collagen IV were larger on average, however the variation in this data precluded statistical significance.

Twitch power, which is the product of the instantaneous twitch force and twitch velocity, has a similar temporal trend as twitch velocity. Prior to contraction the power is zero. In the contraction phase, the twitch power reaches a maximum value, and then reduces back down to zero. A relaxation phase follows, during which the twitch power reaches a minimum (maximum negative) value of power, and then rises back up to zero (Figs. 4(*a*)–4(*c*): fibronectin, laminin, and collagen IV). We noted that maximum contraction power is reached after maximum contraction velocity, but prior to maximum force. Similarly, we observed that maximum relaxation power is reached before maximum relaxation velocity, but after maximum force. Upon quantifying data obtained from power curves for cells on each of the three ECM proteins, we found no significant differences in contraction power (averaging 19–41 fW) or relaxation power (averaging 18–35 fW). Similar to velocity, cells on collagen IV tended to produce the most power, but large variances in this data barred statistical significance (Figs. 4(*d*) and 4(*e*)).

Attachment and Spread Area. Previously, researchers have found that early-stage stem cell-derived cardiomyocytes exhibit an unspread, spherical shape when replated onto tissue culture surfaces, which subsequently results in a low degree of cell attachment. The effectiveness of the micropost platform is dependent on the number of cells attached and spread on top of the microposts. Therefore, in order for this system to effectively yield the contractile properties of stem cell-derived cardiomyocytes, the microposts need to allow for a high degree of cell attachment and spreading. To determine whether the stamped protein had any effect on these properties, cell counts were taken from substrates stamped with fibronectin, laminin, and collagen IV, and the spread areas of these attached cells were measured. On average, there were 13–20 microposts underneath each cell (Figs. 5(*a*)–5(*c*): fibronectin, laminin, and collagen IV). While hiPSC-CMs attached to all three of the ECM proteins, a significantly higher percentage of cells adhered onto microposts stamped with laminin than to those stamped with fibronectin or collagen IV (Fig. 5(*d*)). This same trend also held for cell spread area (Fig. 5(*e*)).

Sarcomeric Structure. As a cardiomyocyte matures, its cross-sectional area transitions from a circular to a rectangular shape. Along with this shape change, the cell's sarcomeres grow in length, becoming perpendicularly aligned to the long axis of the

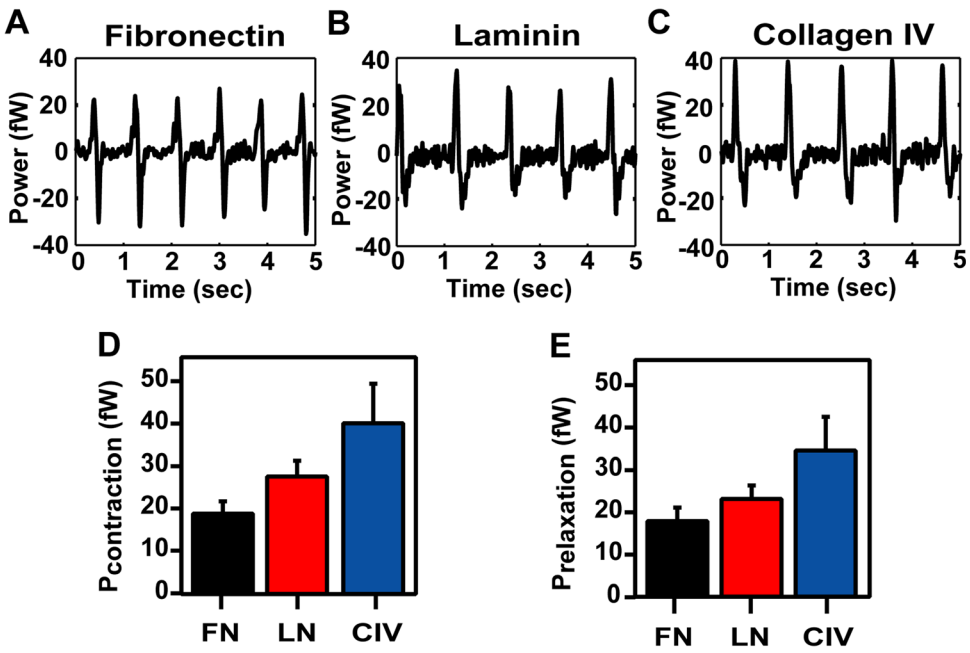

Fig. 4 Twitch power representative power traces for cells seeded on fibronectin (*a*), laminin (*b*), and collagen IV (*c*) demonstrate the ability of this technique to effectively resolve the contraction and relaxation power produced by hiPSC-CMs. Quantification of these power traces revealed higher overall contraction and relaxation velocities for cells on collagen IV, but no significant difference between any of the treatments (*d*) and (*e*).

cell, and the spacing between parallel Z-bands increases. These structural changes lead to increases in the ability of cells to produce contractile force in accordance with the Frank–Starling mechanism [54]. At the same time that these changes are occurring, the percentage of multinucleated cells also increases. Upon analyzing immunofluorescent images of cells on all three ECM proteins (Figs. 5(*a*)–5(*c*)), we found no significant differences in circularity (Fig. 5(*f*)), Z-band width, sarcomere length (Fig. 5(*h*)), or multinucleation (Fig. 5(*i*)).

Discussion

This work demonstrates that micropost arrays can be used to analyze the passive tension, as well as the twitch force, velocity, and power of single iPSC-derived cardiomyocytes. Furthermore, we demonstrated that all of the posts under a cell can be analyzed with sufficient temporal resolution to determine the maxima in these values. Additionally, we established that this technique is compatible with immunofluorescent staining, which enables the visualization of cytoskeletal organization and maturation, as well as measurements of cell hypertrophy and nucleation. Using these techniques, we found that hiPSC-CMs seeded onto laminin demonstrated significantly higher attachment and spread area, as well as higher contraction and relaxation velocities, than those seeded onto fibronectin or collagen IV. These findings indicate that the laminin coating resulted in better adherence between the hiPSC-CMs and the microposts, and may also have led to enhanced contractile maturation.

The cardiac ECM is a dynamic structural entity, with an interstitium principally composed of collagen I, collagen III, and proteoglycans and a basement membrane primarily composed of fibronectin, collagen IV, laminin, entactin, and proteoglycans [54,55]. Previous studies have found that cells can attach to a variety of different substrates and coatings, but that only a handful of these have the right macromolecule surface to elicit long-term cell attachment and spreading [32,46–48]. Specifically, neonatal cardiomyocytes were found to attach to collagens I through IV, fibronectin, and laminin, whereas adult cardiomyocytes preferentially adhere to laminin and collagen IV [32,46–48]. Furthermore, adult cardiomyocytes were unable to attach to collagen I, II, III, or V, and had very low attachment on fibronectin [32,46,47]. Therefore, our findings that hiPSC-CMs attach to and spread to a greater degree on laminin, than on fibronectin or collagen IV, support the notion that these cells exhibit "adult-like" characteristics with regard to their recognition of ECM components.

Recognition, attachment, and survival of cells on surfaces coated with different matrix proteins is governed by integrins, which initiate intracellular signaling cascades and serve as physical links between the ECM and a cell's cytoskeleton [54,56,57]. Integrins are heterodimeric receptors composed of α and β subunits [58], and the pairing of these subunits results in a specificity towards different ECM proteins [57]. Cardiomyocytes primarily express β_1-specific integrins that bind to the fibronectin ($\alpha_3\beta_1$, $\alpha_5\beta_1$, $\alpha_v\beta_1$, and $\alpha_9\beta_1$), laminin ($\alpha_1\beta_1$, $\alpha_3\beta_1$, $\alpha_6\beta_1$, and $\alpha_7\beta_1$), and collagen IV ($\alpha_1\beta_1$, $\alpha_3\beta_1$, and $\alpha_{10}\beta_1$), as well as β_3 and β_5 subunits, whose specificity for these ECM proteins is largely unknown [46,55–58]. Neonatal cardiomyocytes express α_1, α_3, α_5, α_6, and α_7 chains, whereas adult myocytes have no expression of α_1, low expression of α_3 and α_6, and high expression of α_7 [46,56,58,59]. Alternatively, human embryonic stem cell-derived cardiomyocytes were found to express the α_3, α_5, α_6, α_7, α_v, and β_1 integrin subunits, while the α_1, α_2, α_4, and α_{10} subunits were absent [60]. The presence of other alpha chains in neonate and adult cardiomyocytes and the integrin expression for hiPSC-CMs have not been previously investigated. However, these studies indicate that integrin expression within cardiomyocytes changes during development, and suggest there are similarities in integrin expression between adult myocytes and stem cell-derived cardiomyocytes. Similar findings were discovered in the present study. In order to better understand the relationship between hiPSC-CMs and their underlying ECM protein, these cells should be stained for specific integrin subunits in future studies.

Previous studies that assessed the contractile characteristics of single stem cell-derived cardiomyocytes report twitch forces in the range of 0.1 nN to 144 nN, depending on the stiffness of the underlying substrate, the technique used to acquire these values,

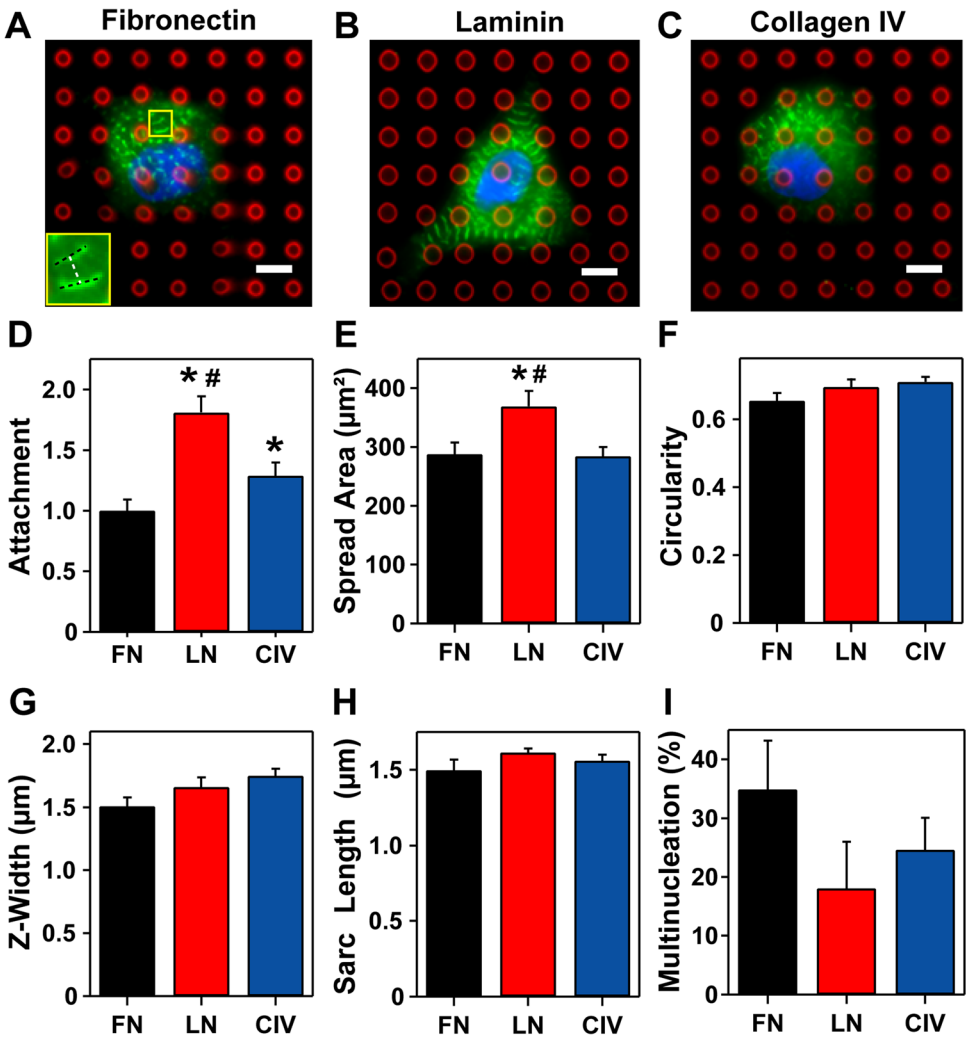

Fig. 5 Maturation Immunofluorescent imaging of hiPSC-CMs seeded onto fibronectin (*a*), laminin (*b*), and collagen IV (*c*) coated microposts revealed punctate, unorganized sarcomeres within cells on fibronectin and collagen IV post, and more highly organized sarcomere structure within cells on laminin posts. Here, α-actinin is indicated by green, the cell nuclei is blue, and the microposts are red. The figure inset demonstrates how measurements of sarcomere length (dark dashed line) and Z-band width (light dashed line) were performed, Cell attachment (*d*) and spread area (*e*) are significantly higher on laminin posts than fibronectin posts, as well as attachment is significantly higher on laminin when compared to collagen IV. The circularity (*f*), Z-band widths (*g*), sarcomere lengths (*h*), and percentage of multinucleated cells (*i*) of the cells was not significantly different based on treatment. Color figures are available in the online version of this publication. Scale bar indicates 6 μm.

and whether or not the cells were electrically stimulated [27,45,61–63]. In general, smaller twitch forces are reported using an AFM, whereas the largest forces are found using traction force microscopy. We found that hiPSC-CMs produced an average twitch force of 13.3 nN to 17.6 nN, which falls within this established range. Using micropost arrays, Taylor et al. found an average twitch force of around 50 nN for cells on 27 μm-diameter posts [45]. However, it is unclear whether or not these values came from single cells or groups of cells. In general, groups of cells beat with more force than single cells, so this could account for the discrepancy in values obtained by the Pruitt group and our own [27]. Nevertheless, all of these values of force are substantially lower than those measured for adult rat cardiomyocytes, which have been found to produce twitch forces within the range of 0.73 μN to 12.6 μN [21,23,64,65]. Therefore, the contractile properties of hiPSC-CMs are still very immature in nature, and require further maturation to replace, or to serve as a model for, adult cardiomyocytes. Additionally, we found no statistical differences in the forces measured for hiPSC-CMs on posts coated with different ECM proteins, on neither a twitch force nor force per area basis. Similarly, upon investigating the passive force produced by individual hiPSC-CMs on different ECMs, we found an average force of 40.7 nN, with no statistical differences between the three conditions. Passive force (or tension) is an important factor in cardiac muscle because it determines the extent to which the heart fills—which dictates the stroke volume—and has been shown to have an effect on cardiomyocyte shortening velocity [66]. This tension is primarily governed by the sarcomeric protein titin, which acts like a mechanical spring, and has been found to have an altered isoform in ischemic heart disease [67,68]. Therefore, passive tension, assessed via arrays of microposts, could be used as a means to distinguish differences between wild-type and disease cell lines.

The average twitch velocity of early-stage (20–40 days post-differentiation) hiPSC-derived cardiomyocytes has previously been measured to be approximately 2 μm/s, based on optical edge detection, while the twitch velocity of midstage (40–60 days post-differentiation) cells was approximately 3 μm/s [69].

Alternatively, using traction force microcopy, the average twitch velocity of midstage hESC-derived cardiomyocytes on a 4 kPa gel was measured to be approximately 6.9 μm/s [62]. Using micropost arrays, we found that the average contraction twitch velocity of early-stage hiPSC-derived cardiomyocytes fell within the range of 1.4–2.0 μm/s, while the relaxation velocity averaged values between 1.2 and 1.6 μm/s. These values are similar to those previously found for hESC and hiPSC derived cardiomyocytes, as well as they are similar to those found for adult cardiomyocytes using Ionoptix (3–5 μm/s contraction velocity and 2–4 μm/s relaxation velocity), but they are much lower than those found for adult cardiomyocytes using carbon fibers ($\sim$107 μm/s) [23].

To the best of our knowledge, there have been no other previous studies that have investigated the power produced by stem cell-derived cardiomyocytes. We measured the average maximum contraction twitch power of early to midstage hiPSC-CMs to fall within the range of 19–41 fW, and relaxation power to be between 18 and 35 fW. However, the maximum twitch power of neonate rat cardiomyocytes has been found to fluctuate between 75 and 200 fW [43], while adult cardiomyocytes can generate around 25 pW of power [70]. Therefore, these results further substantiate that the contractile properties of these cells are still fairly immature in comparison to adult cardiomyocytes. Furthermore, we found that the average beat frequency of hiPSC-CMs on microposts coated with all three ECM proteins was approximately equal, and only varied from 0.9 to 1.1 Hz. These findings agree with previous measurements of the spontaneous beating rate for early-stage iPSC-derived cardiomyocytes, but these values are slightly higher than the spontaneous beating rate for adult cells [27,63,69]. However, these results should be confirmed with paced cells to assess the effect of pacing on cytoskeletal organization and maturation, as well as on the contractile properties of these cells.

As a cardiomyocyte matures from the embryonic to the adult state, its spread area increases, and its shape transitions from a circular to an elongated anisotropic morphology, both of which contribute to higher contractile forces. This increase in cell size is accompanied by an increase in the number of contractile proteins within the cell [71], while the shape transition leads to an enhanced alignment and organization of these proteins [72]. The average spread area of early-stage stem cell-derived cardiomyocytes on flat surfaces has previously been measured to fall within the range of 480–1200 μm^2, depending on the stiffness of the underlying substrate [17,73]. Here, we found that the average spread area for hiPSC-CMs on microposts was $287.62 \pm 20.12\ \mu m^2$ for cells on fibronectin coatings, $368.56 \pm 26.34\ \mu m^2$ for cells on laminin coatings, and $284.53 \pm 15.50\ \mu m^2$ for cells on collagen IV coatings. These results demonstrate that laminin-coated posts yield cell spread areas that most closely replicate those found for early-stage stem cell-derived cardiomyocytes on flat surfaces; however, these values are still much smaller than that of an adult cardiomyocyte, which varies from around 1000 to 1500 μm^2 [55]. Additionally, the average circularity of early-stage, stem cell-derived cardiomyocytes has previously been measured to vary from 0.38 to 0.6 [17,73], whereas we found average circularities within the range 0.65–0.71. This discrepancy in cell geometry could be due partially to the lower degree of spreading on microposts arrays for hiPSC-CMs and to the limited adhesive geometry of the micropost arrays. Overall, these results suggest that strategies for improving the spread area and alignment of hiPSC-CMs on arrays of microposts should be included in future research efforts in order to further enhance the structural maturation of these cells.

The sarcomere is the fundamental structural unit involved in force generation within cardiomyocytes. During development, sarcomeres grow in length and align in the direction perpendicular to the long-axis of the cell, and the Z-band distance between parallel sarcomeres increases. The increased length of these sarcomeres indicates an elevated probability of actin-myosin cross-bridge formation [74], and increased Z-band widths indicate enhanced coupling between adjacent sarcomeres [75]; both of which contribute to higher actomyosin forces. In our studies, we found that the average Z-band width for hiPSC-CMs was $1.51 \pm 0.07\ \mu$m for cells on fibronectin posts, $1.66 \pm 0.07\ \mu$m for those on laminin posts, and $1.75 \pm 0.06\ \mu$m for cells on collagen IV posts. While we were unable to find references to Z-band width for stem cell-derived cardiomyocytes, the average Z-band width of a neonate cardiomyocyte can vary from 2.35 to 3.84 μm, and adult Z-band widths can be even larger [43,44]. The average sarcomere length for an early-stage stem cell-derived cardiomyocytes on a flat, gelatin-coated surface is 1.65 μm [73], while those measured for an adult rat fall within the range between 1.53 and 2.4 μm [21,23,64,65,76]. In comparison, we found sarcomere lengths ranging from 1.5 μm to 1.6 μm. These shorter sarcomere lengths and Z-band widths likely contribute to the overall lower force seen in hiPSC-CM cells, when compared to adult cardiomyocytes.

Lastly, previous work has found that the multinucleation percentage of early-stage stem cell-derived cardiomyocytes is around 4.2% [73]. We found multinucleation percentages of $35 \pm 8\%$ for fibronectin, $18 \pm 8\%$ for laminin, and $25 \pm 5\%$ for collagen IV. In the human heart, the percentage of multinucleated cells increases from the neonatal stage to comprise approximately 26% of the cardiomyocytes in the adult human heart, while the other 74% of these cells remain mononucleated [77]. Therefore, collagen IV-stamped posts yielded multinucleation percentages that most closely mimic those seen in the adult heart, while laminin coatings resulted in fewer multinucleated cells, and fibronectin coatings resulted in extra multinucleated cells. However, all of these values are much larger than those previously seen for early-stage stem cell-derived cardiomyocytes.

Conclusion

Here, we reported the development of a platform technology for the assessment of hiPSC-CM contractility. We demonstrated that this platform is able to effectively measure the twitch force, velocity, and power at all points of adhesion underneath a cell and is compatible with immunofluorescent staining. Therefore, this technology could be used to determine quantifiable differences in contractility between populations of hiPSC-CMs that are from: (i) cultures of different developmental states, (ii) patients with heart disease, (iii) different differentiation or culture protocols, (iv) virally or chemically treated cultures, or (v) cultures exposed to different external stimuli. Thus, this technique has the potential to serve as a very powerful tool within the field of heart mechanics. However, it is not without its limitations. As demonstrated by this study, the cell area and elongation of hiPSC-CMs on microposts are reduced when compared to those on flat culture surfaces. Additionally, in its current configuration, this system does not allow for electrical or mechanical stimulation, which are both essential to heart maturation and maintenance in vivo. Finally, because this technique relies upon optical means to track the location of posts over time, the temporal resolution of the measurements is limited by the speed of the camera used to acquire them. Therefore, future research efforts will focus on amending these shortcomings. The results of this particular study suggest that, in future experiments, the microposts should be stamped with laminin to enable the highest degree of cell attachment, spreading, and an enhanced degree of contractile maturation.

Acknowledgment

The authors wish to acknowledge support from the following sources: an NSF GRFP fellowship awarded to MLR, an NSF REU supplement for BTG, NIH Grant Nos. P01 HL094374, P01 GM081719, U01 HL100405, R01 HL084642, and U01 HL100395 to CEM, and an NSF CAREER grant awarded to NJS. Also, special thanks to Mark Saiget and James Fugate at the Murry Lab for their assistance in learning protocols related to hiPSC-CM production. Part of this work was conducted at the University of

Washington Microfabrication/Nanotechnology User Facility, a member of the NSF National Nanotechnology Infrastructure Network.

Conceived and designed the experiments: MLR, NJS. Performed the experiments: MLR. Analyzed the data: MLR, BTG. Contributed reagents/materials/analysis tools: MLR, BTG, LMP, SJH, and CEM. Wrote the Paper: MLR, BTG, NJS, LMP, and CEM.

References

[1] Bonow, R., Mann, D. L., Zipes, D. P., and Libby, P., 2012, *Braunwald's Heart Disease: A Textbook of Cardiovascular Medicine*, Saunders, Philadelphia, PA.

[2] Karantalis, V., Balkan, W., Schulman, I. H., Hatzistergos, K. E., and Hare, J. M., 2012, "Cell-Based Therapy for Prevention and Reversal of Myocardial Remodeling," Am. J. Physiol.: Heart Circ. Physiol., **303**(3), pp. H256–H270.

[3] Suncion, V. Y., Schulman, I. H., and Hare, J. M., 2012, "Concise Review: The Role of Clinical Trials in Deciphering Mechanisms of Action of Cardiac Cell-Based Therapy," Stem Cells Transl. Med., **1**(1), pp. 29–35.

[4] Bellin, M., Marchetto, M. C., Gage, F. H., and Mummery, C. L., 2012, "Induced Pluripotent Stem Cells: The New Patient?," Nat. Rev. Mol. Cell Biol., **13**(11), pp. 713–726.

[5] Grskovic, M., Javaherian, A., Strulovici, B., and Daley, G. Q., 2011, "Induced Pluripotent Stem Cells-Opportunities for Disease Modelling and Drug Discovery," Nat. Rev. Drug Discov., **10**(12), pp. 915–929.

[6] Dambrot, C., Passier, R., Atsma, D., and Mummery, C. L., 2011, "Cardiomyocyte Differentiation of Pluripotent Stem Cells and Their Use as Cardiac Disease Models," Biochem. J., **434**(1), pp. 25–35.

[7] Das, A. K., and Pal, R., 2010, "Induced Pluripotent Stem Cells (Ipscs): The Emergence of a New Champion in Stem Cell Technology-Driven Biomedical Applications," J. Tissue Eng. Regener. Med., **4**(6), pp. 413–421.

[8] Freund, C., and Mummery, C. L., 2009, "Prospects for Pluripotent Stem Cell-Derived Cardiomyocytes in Cardiac Cell Therapy and as Disease Models," J. Cell. Biochem., **107**(4), pp. 592–599.

[9] Mercola, M., Colas, A., and Willems, E., 2013, "Induced Pluripotent Stem Cells in Cardiovascular Drug Discovery," Circ. Res., **112**(3), pp. 534–548.

[10] Miki, K., Uenaka, H., Saito, A., Miyagawa, S., Sakaguchi, T., Higuchi, T., Shimizu, T., Okano, T., Yamanaka, S., and Sawa, Y., 2012, "Bioengineered Myocardium Derived From Induced Pluripotent Stem Cells Improves Cardiac Function and Attenuates Cardiac Remodeling Following Chronic Myocardial Infarction in Rats," Stem Cells Transl. Med., **1**(5), pp. 430–437.

[11] Kawamura, M., Miyagawa, S., Miki, K., Saito, A., Fukushima, S., Higuchi, T., Kawamura, T., Kuratani, T., Daimon, T., Shimizu, T., Okano, T., and Sawa, Y., 2012, "Feasibility, Safety, and Therapeutic Efficacy of Human Induced Pluripotent Stem Cell-Derived Cardiomyocyte Sheets in a Porcine Ischemic Cardiomyopathy Model," Circulation, **126**(11 Suppl 1), pp. S29–S37.

[12] Masumoto, H., Matsuo, T., Yamamizu, K., Uosaki, H., Narazaki, G., Katayama, S., Marui, A., Shimizu, T., Ikeda, T., Okano, T., Sakata, R., and Yamashita, J. K., 2012, "Pluripotent Stem Cell-Engineered Cell Sheets Reassembled With Defined Cardiovascular Populations Ameliorate Reduction in Infarct Heart Function Through Cardiomyocyte-Mediated Neovascularization," Stem Cells, **30**(6), pp. 1196–1205.

[13] Mauritz, C., Martens, A., Rojas, S. V., Schnick, T., Rathert, C., Schecker, N., Menke, S., Glage, S., Zweigerdt, R., Haverich, A., Martin, U., and Kutschka, I., 2011, "Induced Pluripotent Stem Cell (iPSC)-Derived Flk-1 Progenitor Cells Engraft, Differentiate, and Improve Heart Function in a Mouse Model of Acute Myocardial Infarction," Eur. Heart J., **32**(21), pp. 2634–2641.

[14] Singla, D. K., Long, X., Glass, C., Singla, R. D., and Yan, B., 2011, "Induced Pluripotent Stem (IPS) Cells Repair and Regenerate Infarcted Myocardium," Mol. Pharm., **8**(5), pp. 1573–1581.

[15] Mosna, F., Annunziato, F., Pizzolo, G., and Krampera, M., 2010, "Cell Therapy for Cardiac Regeneration After Myocardial Infarct: Which Cell Is the Best?," Cardiovasc. Hematol. Agents Med. Chem., **8**(4), pp. 227–243.

[16] Yin, S., Zhang, X., Zhan, C., Wu, J., Xu, J., and Cheung, J., 2005, "Measuring Single Cardiac Myocyte Contractile Force Via Moving a Magnetic Bead," Biophys. J., **88**(2), pp. 1489–1495.

[17] Hazeltine, L. B., Simmons, C. S., Salick, M. R., Lian, X., Badur, M. G., Han, W., Delgado, S. M., Wakatsuki, T., Crone, W. C., Pruitt, B. L., and Palecek, S. P., 2012, "Effects of Substrate Mechanics on Contractility of Cardiomyocytes Generated From Human Pluripotent Stem Cells," Int. J. Cell Biol., **2012**, p. 508294.

[18] Hersch, N., Wolters, B., Dreissen, G., Springer, R., Kirchgebner, N., Merkel, R., and Hoffmann, B., 2013, "The Constant Beat: Cardiomyocytes Adapt Their Forces by Equal Contraction Upon Environmental Stiffening," Biol. Open, **2**, pp. 351–361.

[19] Jacot, J. G., Mcculloch, A. D., and Omens, J. H., 2008, "Substrate Stiffness Affects the Functional Maturation of Neonatal Rat Ventricular Myocytes," Biophys. J., **95**(7), pp. 3479–3487.

[20] Jacot, J. G., Martin, J. C., and Hunt, D. L., 2010, "Mechanobiology of Cardiomyocyte Development," J. Biomech., **43**(1), pp. 93–98.

[21] Iribe, G., Helmes, M., and Kohl, P., 2007, "Force-Length Relations in Isolated Intact Cardiomyocytes Subjected to Dynamic Changes in Mechanical Load," Am. J. Physiol.: Heart Circ. Physiol., **292**(3), pp. H1487–H1497.

[22] Borbely, A., Van Der Velden, J., Papp, Z., Bronzwaer, J. G., Edes, I., Stienen, G. J., and Paulus, W. J., 2005, "Cardiomyocyte Stiffness in Diastolic Heart Failure," Circulation, **111**(6), pp. 774–781.

[23] Nishimura, S., Yasuda, S., Katoh, M., Yamada, K. P., Yamashita, H., Saeki, Y., Sunagawa, K., Nagai, R., Hisada, T., and Sugiura, S., 2004, "Single Cell Mechanics of Rat Cardiomyocytes Under Isometric, Unloaded, and Physiologically Loaded Conditions," Am. J. Physiol.: Heart Circ. Physiol., **287**(1), pp. H196–H202.

[24] Nishimura, S., Nagai, S., Sata, M., Katoh, M., Yamashita, H., Saeki, Y., Nagai, R., and Sugiura, S., 2006, "Expression of Green Fluorescent Protein Impairs the Force-Generating Ability of Isolated Rat Ventricular Cardiomyocytes," Mol. Cell. Biochem., **286**(1–2), pp. 59–65.

[25] Domke, J., Parak, W. J., George, M., Gaub, H. E., and Radmacher, M., 1999, "Mapping the Mechanical Pulse of Single Cardiomyocytes With the Atomic Force Microscope," Eur. Biophys. J., **28**(3), pp. 179–186.

[26] Chang, W. T., Yu, D., Lai, Y. C., Lin, K. Y., and Liau, I., 2012, "Characterization of the Mechanodynamic Response of Cardiomyocytes With Atomic Force Microscopy," Anal. Chem., **85**, pp. 1395–1400.

[27] Liu, J., Sun, N., Bruce, M. A., Wu, J. C., and Butte, M. J., 2012, "Atomic Force Mechanobiology of Pluripotent Stem Cell-Derived Cardiomyocytes," PLoS One, **7**(5), p. e37559.

[28] Brixius, K., Hoischen, S., Reuter, H., Lasek, K., and Schwinger, R. H., 2001, "Force/Shortening-Frequency Relationship in Multicellular Muscle Strips and Single Cardiomyocytes of Human Failing and Nonfailing Hearts," J. Card. Failure, **7**(4), pp. 335–341.

[29] Edes, I. F., Czuriga, D., Csanyi, G., Chlopicki, S., Recchia, F. A., Borbely, A., Galajda, Z., Edes, I., Van Der Velden, J., Stienen, G. J. M., and Papp, Z., 2007, "Rate of Tension Redevelopment Is Not Modulated by Sarcomere Length in Permeabilized Human, Murine, and Porcine Cardiomyocytes," Am. J. Physiol.: Regul., Integr. Comp. Physiol., **293**(1), pp. R20–R29.

[30] Tanaka, Y., Morishima, K., Shimizu, T., Kikuchi, A., Yamato, M., Okano, T., and Kitamori, T., 2006, "Demonstration of a PDMS-Based Bio-Microactuator Using Cultured Cardiomyocytes to Drive Polymer Micropillars," Lab Chip, **6**(2), pp. 230–235.

[31] Vannier, C., Chevassus, H., and Vassort, G., 1996, "Ca-Dependence of Isometric Force Kinetics in Single Skinned Ventricular Cardiomyocytes From Rats," Cardiovasc. Res., **32**(3), pp. 580–586.

[32] Borg, T. K., Rubin, K., Lundgren, E., Borg, K., and Obrink, B., 1984, "Recognition of Extracellular Matrix Components by Neonatal and Adult Cardiac Myocytes," Dev. Biol., **104**(1), pp. 86–96.

[33] Xi, J., Khalil, M., Shishechian, N., Hannes, T., Pfannkuche, K., Liang, H., Fatima, A., Haustein, M., Suhr, F., Bloch, W., Reppel, M., Saric, T., Wernig, M., Janisch, R., Brockmeier, K., Hescheler, J., and Pillekamp, F., 2010, "Comparison of Contractile Behavior of Native Murine Ventricular Tissue and Cardiomyocytes Derived From Embryonic or Induced Pluripotent Stem Cells," FASEB J., **24**(8), pp. 2739–2751.

[34] Eschenhagen, T., Fink, C., Remmers, U., Scholz, H., Wattchow, J., Weil, J., Zimmermann, W., Dohmen, H. H., Schafer, H., Bishopric, N., Wakatsuki, T., and Elson, E. L., 1997, "Three-Dimensional Reconstitution of Embryonic Cardiomyocytes in a Collagen Matrix: A New Heart Muscle Model System," FASEB J., **11**(8), pp. 683–694.

[35] Pillekamp, F., Reppel, M., Rubenchyk, O., Pfannkuche, K., Matzkies, M., Bloch, W., Sreeram, N., Brockmeier, K., and Hescheler, J., 2007, "Force Measurements of Human Embryonic Stem Cell-Derived Cardiomyocytes in an in Vitro Transplantation Model," Stem Cells, **25**(1), pp. 174–180.

[36] Kim, J., Park, J., Na, K., Yang, S., Baek, J., Yoon, E., Choi, S., Lee, S., Chun, K., Park, J., and Park, S., 2008, "Quantitative Evaluation of Cardiomyocyte Contractility in a 3D Microenvironment," J. Biomech., **41**(11), pp. 2396–2401.

[37] Park, J., Ryu, J., Choi, S. K., Seo, E., Cha, J. M., Ryu, S., Kim, J., Kim, B., and Lee, S. H., 2005, "Real-Time Measurement of the Contractile Forces of Self-Organized Cardiomyocytes on Hybrid Biopolymer Microcantilevers," Anal. Chem., **77**(20), pp. 6571–6580.

[38] Boudou, T., Legant, W. R., Mu, A., Borochin, M. A., Thavandiran, N., Radisic, M., Zandstra, P. W., Epstein, J. A., Margulies, K. B., and Chen, C. S., 2011, "A Microfabricated Platform to Measure and Manipulate the Mechanics of Engineered Cardiac Microtissues," Tissue Eng. Part A, **18**(9–10), pp. 910–919.

[39] Legant, W. R., Pathak, A., Yang, M. T., Deshpande, V. S., Mcmeeking, R. M., and Chen, C. S., 2009, "Microfabricated Tissue Gauges to Measure and Manipulate Forces From 3D Microtissues," Proc. Natl. Acad. Sci. USA, **106**(25), pp. 10097–10102.

[40] Kim, K., Taylor, R., Sim, J. Y., Park, S. J., Norman, J., Fajardo, G., Bernstein, D., and Pruitt, B. L., 2011, "Calibrated Micropost Arrays for Biomechanical Characterisation of Cardiomyocytes," Micro Nano Lett., **6**(5), pp. 317–322.

[41] Zhao, Y., Lim, C. C., Sawyer, D. B., Liao, R. L., and Zhang, X., 2005, "Cellular Force Measurements Using Single-Spaced Polymeric Microstructures: Isolating Cells From Base Substrate," J. Micromech. Microeng., **15**(9), pp. 1649–1656.

[42] Zhao, Y., and Zhang, X., 2006, "Cellular Mechanics Study in Cardiac Myocytes Using PDMS Pillars Array," Sens. Actuators, A, **125**(2), pp. 398–404.

[43] Rodriguez, A. G., Han, S. J., Regnier, M., and Sniadecki, N. J., 2011, "Substrate Stiffness Increases Twitch Power of Neonatal Cardiomyocytes in Correlation With Changes in Myofibril Structure and Intracellular Calcium," Biophys. J., **101**(10), pp. 2455–2464.

[44] Rodriguez, A. G., Rodriguez, M. L., Han, S. J., Sniadecki, N. J., and Regnier, M., 2013, "Enhanced Contractility With 2 Deoxy-ATP and EMD 57033 Leads to Reduced Myofibril Structure and Twitch Power in Neonatal Cardiomyocytes," Integr. Biol., **5**(11), pp. 1366–1373.

[45] Taylor, R. E., Kim, K., Sun, N., Park, S. J., Sim, J. Y., Fajardo, G., Bernstein, D., Wu, J. C., and Pruitt, B. L., 2013, "Sacrificial Layer Technique for Axial Force Post Assay of Immature Cardiomyocytes," Biomed. Microdevices, **15**(1), pp. 171–181.
[46] Terracio, L., Rubin, K., Gullberg, D., Balog, E., Carver, W., Jyring, R., and Borg, T. K., 1991, "Expression of Collagen Binding Integrins During Cardiac Development and Hypertrophy," Circ. Res., **68**(3), pp. 734–744.
[47] Lundgren, E., Terracio, L., Mardh, S., and Borg, T. K., 1985, "Extracellular Matrix Components Influence the Survival of Adult Cardiac Myocytes in vitro," Exp. Cell Res., **158**(2), pp. 371–381.
[48] Lundgren, E., Terracio, L., and Borg, T. K., 1985, "Adhesion of Cardiac Myocytes to Extracellular Matrix Components," Basic Res. Cardiol., **80**(Suppl 1), pp. 69–74.
[49] Tan, J. L., Tien, J., Pirone, D. M., Gray, D. S., Bhadriraju, K., and Chen, C. S., 2003, "Cells Lying on a Bed of Microneedles: An Approach to Isolate Mechanical Force," Proc. Natl. Acad. Sci. USA, **100**(4), pp. 1484–1489.
[50] Sniadecki, N. J., and Chen, C. S., 2007, "Microfabricated Silicone Elastomeric Post Arrays for Measuring Traction Forces of Adherent Cells," *Methods in Cell Biology: Cell Mechanics*, Elsevier Inc., San Diego, CA.
[51] Yu, J., Vodyanik, M. A., Smuga-Otto, K., Antosiewicz-Bourget, J., Frane, J. L., Tian, S., Nie, J., Jonsdottir, G. A., Ruotti, V., Stewart, R., Slukvin, I., and Thomson, J. A., 2007, "Induced Pluripotent Stem Cell Lines Derived From Human Somatic Cells," Science, **318**(5858), pp. 1917–1920.
[52] Laflamme, M. A., Chen, K. Y., Naumova, A. V., Muskheli, V., Fugate, J. A., Dupras, S. K., Reinecke, H., Xu, C., Hassanipour, M., Police, S., O'Sullivan, C., Collins, L., Chen, Y., Minami, E., Gill, E. A., Ueno, S., Yuan, C., Gold, J., and Murry, C. E., 2007, "Cardiomyocytes Derived From Human Embryonic Stem Cells in Pro-Survival Factors Enhance Function of Infarcted Rat Hearts," Nat. Biotechnol., **25**(9), pp. 1015–1024.
[53] Han, S. J., Bielawski, K. S., Ting, L. H., Rodriguez, M. L., and Sniadecki, N. J., 2012, "Decoupling Substrate Stiffness, Spread Area, and Micropost Density: A Close Spatial Relationship Between Traction Forces and Focal Adhesions," Biophys. J., **103**(4), pp. 640–648.
[54] Kresh, J. Y., and Chopra, A., 2011, "Intercellular and Extracellular Mechanotransduction in Cardiac Myocytes," Pflugers Arch., **462**(1), pp. 75–87.
[55] Parker, K. K., and Ingber, D. E., 2007, "Extracellular Matrix, Mechanotransduction and Structural Hierarchies in Heart Tissue Engineering," Philos. Trans. R. Soc., B, **362**(1484), pp. 1267–1279.
[56] Wu, X., Sun, Z., Foskett, A., Trzeciakowski, J. P., Meininger, G. A., and Muthuchamy, M., 2010, "Cardiomyocyte Contractile Status Is Associated With Differences in Fibronectin and Integrin Interactions," Am. J. Physiol.: Heart Circ. Physiol., **298**(6), pp. H2071–H2081.
[57] Prowse, A. B., Chong, F., Gray, P. P., and Munro, T. P., 2011, "Stem Cell Integrins: Implications for ex-Vivo Culture and Cellular Therapies," Stem Cell Res., **6**(1), pp. 1–12.
[58] Ross, R. S., and Borg, T. K., 2001, "Integrins and the Myocardium," Circ. Res., **88**(11), pp. 1112–1119.
[59] Maitra, N., Flink, I. L., Bahl, J. J., and Morkin, E., 2000, "Expression of Alpha and Beta Integrins During Terminal Differentiation of Cardiomyocytes," Cardiovasc. Res., **47**(4), pp. 715–725.
[60] Van Laake, L. W., Van Donselaar, E. G., Monshouwer-Kloots, J., Schreurs, C., Passier, R., Humbel, B. M., Doevendans, P. A., Sonnenberg, A., Verkleij, A. J., and Mummery, C. L., 2010, "Extracellular Matrix Formation After Transplantation of Human Embryonic Stem Cell-Derived Cardiomyocytes," Cell. Mol. Life Sci., **67**(2), pp. 277–290.
[61] Wang, I. N., Wang, X., Ge, X., Anderson, J., Ho, M., Ashley, E., Liu, J., Butte, M. J., Yazawa, M., Dolmetsch, R. E., Quertermous, T., and Yang, P. C., 2012, "Apelin Enhances Directed Cardiac Differentiation of Mouse and Human Embryonic Stem Cells," PLoS One, **7**(6), e38328.
[62] Kita-Matsuo, H., Barcova, M., Prigozhina, N., Salomonis, N., Wei, K., Jacot, J. G., Nelson, B., Spiering, S., Haverslag, R., Kim, C., Talantova, M., Bajpai, R., Calzolari, D., Terskikh, A., Mcculloch, A. D., Price, J. H., Conklin, B. R., Chen, H. S., and Mercola, M., 2009, "Lentiviral Vectors and Protocols for Creation of Stable hESC Lines for Fluorescent Tracking and Drug Resistance Selection of Cardiomyocytes," PLoS One, **4**(4), e5046.
[63] Sun, N., Yazawa, M., Liu, J., Han, L., Sanchez-Freire, V., Abilez, O. J., Navarrete, E. G., Hu, S., Wang, L., Lee, A., Pavlovic, A., Lin, S., Chen, R., Hajjar, R. J., Snyder, M. P., Dolmetsch, R. E., Butte, M. J., Ashley, E. A., Longaker, M. T., Robbins, R. C., and Wu, J. C., 2012, "Patient-Specific Induced Pluripotent Stem Cells as a Model for Familial Dilated Cardiomyopathy," Sci. Transl. Med., **4**(130), 130ra47.
[64] Lin, G., Pister, K. S. J., and Roos, K. P., 2000, "Surface Micromachined Polysilicon Heart Cell Force Transducer," J. Microelectromech. Syst., **9**(1), pp. 9–17.
[65] Yasuda, S. I., Sugiura, S., Kobayakawa, N., Fujita, H., Yamashita, H., Katoh, K., Saeki, Y., Kaneko, H., Suda, Y., Nagai, R., and Sugi, H., 2001, "A Novel Method to Study Contraction Characteristics of a Single Cardiac Myocyte Using Carbon Fibers," Am. J. Physiol.: Heart Circ. Physiol., **281**(3), pp. H1442–H1446.
[66] Granzier, H. L., and Irving, T. C., 1995, "Passive Tension in Cardiac Muscle: Contribution of Collagen, Titin, Microtubules, and Intermediate Filaments," Biophys. J., **68**(3), pp. 1027–1044.
[67] Kass, D. A., Bronzwaer, J. G. F., and Paulus, W. J., 2004, "What Mechanisms Underlie Diastolic Dysfunction in Heart Failure?," Circ. Res., **94**(12), pp. 1533–1542.
[68] Hamdani, N., Kooij, V., Van Dijk, S., Merkus, D., Paulus, W. J., Dos Remedios, C., Duncker, D. J., Stienen, G. J. M., and Van Der Velden, J., 2008, "Sarcomeric Dysfunction in Heart Failure," Cardiovasc. Res., **77**(4), pp. 649–658.
[69] Shinozawa, T., Imahashi, K., Sawada, H., Furukawa, H., and Takami, K., 2012, "Determination of Appropriate Stage of Human-Induced Pluripotent Stem Cell-Derived Cardiomyocytes for Drug Screening and Pharmacological Evaluation in Vitro," J. Biomol. Screen, **17**(9), pp. 1192–1203.
[70] Korte, F. S., and McDonald, K. S., 2007, "Sarcomere Length Dependence of Rat Skinned Cardiac Myocyte Mechanical Properties: Dependence on Myosin Heavy Chain," J. Physiol., **581**(Pt 2), pp. 725–739.
[71] Spach, M. S., Heidlage, J. F., Barr, R. C., and Dolber, P. C., 2004, "Cell Size and Communication: Role in Structural and Electrical Development and Remodeling of the Heart," Heart Rhythm, **1**(4), pp. 500–515.
[72] Feinberg, A. W., Alford, P. W., Jin, H., Ripplinger, C. M., Werdich, A. A., Sheehy, S. P., Grosberg, A., and Parker, K. K., 2012, "Controlling the Contractile Strength of Engineered Cardiac Muscle by Hierarchal Tissue Architecture," Biomaterials, **33**(23), pp. 5732–5741.
[73] Lundy, S. D., Zhu, W. Z., Regnier, M., and Laflamme, M. A., 2013, "Structural and Functional Maturation of Cardiomyocytes Derived From Human Pluripotent Stem Cells," Stem Cells Dev., **22**(14), pp. 1991–2002.
[74] Gordon, A. M., Homsher, E., and Regnier, M., 2000, "Regulation of Contraction in Striated Muscle," Physiol. Rev., **80**(2), pp. 853–924.
[75] Campbell, K. S., 2009, "Interactions Between Connected Half-Sarcomeres Produce Emergent Mechanical Behavior in a Mathematical Model of Muscle," PLoS Comput. Biol., **5**(11), e1000560.
[76] Walker, C. A., and Spinale, F. G., 1999, "The Structure and Function of the Cardiac Myocyte: A Review of Fundamental Concepts," J. Thorac. Cardiovasc. Surg., **118**(2), pp. 375–382.
[77] Olivetti, G., Cigola, E., Maestri, R., Corradi, D., Lagrasta, C., Gambert, S. R., and Anversa, P., 1996, "Aging, Cardiac Hypertrophy and Ischemic Cardiomyopathy Do Not Affect the Proportion of Mononucleated and Multinucleated Myocytes in the Human Heart," J. Mol. Cell. Cardiol., **28**(7), pp. 1463–1477.